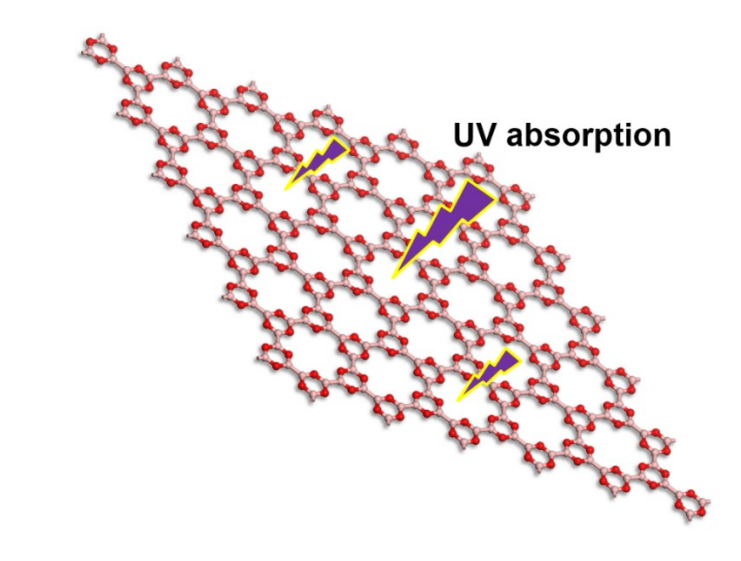
Porous Hexagonal Boron Oxide Monolayer with Robust Wide Band Gap: A Computational Study

Shiru Lin,[†] Jinxing Gu,[†] Haijun Zhang,[‡] Yu Wang, [§] Zhongfang Chen^{†,*} † Department of Chemistry, University of Puerto Rico, Rio Piedras Campus, San Juan, PR 00931, USA [‡] School of Physics and Materials Science, Anhui University, Hefei 230601, China § College of Chemistry and Materials Science, Jiangsu Key Laboratory of Biofunctional Materials, Nanjing Normal University, Nanjing, Jingsu, 210023, China. To whom correspondence should be addressed. Email: <u>zhongfangchen@gmail.com</u> (ZC)

Abstract

By means of density functional theory (DFT) computations, we designed porous hexagonal boron oxide (ph-BO) monolayer, which is purely planar, and has uniform pores in diameter of 6.27 Å. Its high binding energy, absence of imaginary phonon dispersions, and outstanding thermal stability suggest that it is possible to synthesize ph-BO monolayer experimentally. Interestingly, ph-BO is an indirect semiconductor with a rather wide band gap (5.23 eV) comparable to hexagonal boron nitride, and its band gap is rather robust against external strains. ph-BO is promising for many applications because of its exceptional electronic and optical properties, especially in the deep-UV range.

TOC



1. Introduction

Since the experimental realization of graphene in 2004,¹ numerous two-dimensional (2D) materials beyond graphene have been extensively investigated,²⁻¹⁰ including those made of single elements, such as group IV silicene,¹¹⁻¹⁸ germanene,¹⁹⁻²⁴ and stanene,^{5,25-28} group V phosphorene,²⁹⁻³⁵ arsenene³⁶⁻³⁸ and antimonene.^{36,38-42} These new materials not only greatly enriched the 2D materials family, but also revolutionized modern physics, chemistry and materials science, among others. However, most 2D materials have narrow band gaps less than 2.0 eV, which seriously hinder the applications of 2D materials in blue- and UV-light range. Therefore, it is of great importance to theoretically or experimentally search for stable semiconducting 2D materials with wide band gaps.

The group III monolayers did not escape the attention. The structures and electronic properties of 2D nanosheet of boron, namely borophene, have been extensively investigated, 43-50 and recently have been grown on Ag(111) substrates. 51-52

Boron can easily form oxides in nature. Boron oxides have three common forms: boron monoxide (B₂O₃), boron suboxide (B₆O) and boron trioxide (B₂O₃). The high-pressure syntheses of graphite-like⁵³ and diamond-like⁵⁴ structures of B₂O have been reported, however, later experimental⁵⁵ and theoretical⁵⁶ investigations showed that the graphite-like structure is not stable. B₆O is built of eight icosahedra, which are at the apexes of the rhombohedral unit cell, and displays great hardness and high chemical inertness.⁵⁷ B₂O₃ is the most ordinary form of boron oxide in nature. Glass boron trioxide $(g-B_2O_3)^{58}$ is one of the best glass-formers,⁵⁹ in which the

six-membered boroxol rings (B₃O₃) consisting of alternating 3-coordinate boron and 2-coordinate oxygen are supposed to be the building blocks. ^{60,61} However, g-B₂O₃ is lack of low-pressure polymorphism, its crystallization has never been succeeded from a dry melt at ambient pressure so far. Interestingly, Ferlat *et al.* computationally designed some new low-pressure B₂O₃ polymorphs using BO₃ triangle and B₃O₆ boroxol rings. ⁵⁹ The sublattices of these new B₂O₃ polymorphs are flat, and can be considered as B₂O₃ monolayers with BO₃ and B₃O₆ triangle units (Figure S2, see Supporting Information).

Experimentally, Al₂O₃ protecting boron oxide thin films by atomic layer deposition method using BBr₃ and H₂O as precursors,⁶² and boron oxide nanowires by infrared irradiation of B and B₂O₃ powders on Mg metal surface⁶³ have already been realized, though these nanostructures are unstable with respect to moist air, and it was found that upon heating in the absence of air boron oxide can transform to boron-only nanowires.⁶⁴ Moreover, the bulk boron oxides have been used as catalysts⁶⁵ and protective surface treatments.⁶⁶ However, there is sparse work focusing on boron oxide 2D materials.

Recently, King and his coworkers proposed that the planar boron monoxide clusters $(B_nO_n)^{67}$ would be energetically more favorable than the twisted ones when the number of boron monoxide dimer is over 18 (n > 18).⁶⁸ Using the same B_6O_6 dimer as building block, $(B_2O_2)_n$ double-ring tubular clusters⁶⁹ and boroxine based buckyballs and cages⁷⁰ have been theoretical studied. On the other hand, Yang and his coworker reported B_4O 2D semiconductor and B_6O 2D Dirac nodeline semimetal.⁷¹

The extraordinary advances of 2D materials and the purely planar structures of B_nO_n clusters inspired us to answer the following questions: can we construct boron monooxide 2D materials using such building blocks? would they possess rather high stability and have wide band gaps?

Herein, by means of systematic density functional theory computations (DFT) computations, we theoretically designed a 2D material, namely porous hexagonal boron oxide (*ph*-BO), which is a wide band gap semiconductor. Our computations showed that this monolayer is of rather high thermodynamic, dynamic and thermal stabilities, and it is the global minimum among boron monoxide 2D materials. *ph*-BO also has rather robust mechanical strength and efficient absorption in deep-UV light range. All the exceptional properties endow the porous *ph*-BO monolayer promising applications in electronics and optoelectronics.

2. Computation Methods

Our DFT computations were performed using a plane wave basis set with the projector-augmented plane wave $(PAW)^{72}$ to model the ion-electron interaction as implemented in the Vienna ab initio simulation package $(VASP)^{.73}$. The electron exchange-correlation functional was treated using generalized gradient approximation (GGA) in the form proposed by Perdew, Burke and Ernzerhof (PBE). The energy cutoff for ph-BO monolayer was set to 500 eV. The vacuum space is more than 10 Å, so that the interactions between adjacent layers can be ignored. The $9\times9\times1$ Monkhost-Pack k points and 10^{-5} eV convergence tolerances were used for geometry optimizations, self-consistent calculations and electronic calculations. We carried out

both spin-polarized and spin-unpolarized computations and ensured that ph-BO has no magnetism.

Since PBE functional tends to underestimate the band gaps, while the Heyd-Scuseria-Ernzerhof (HSE06)⁷⁴ screened-hybrid functional was proven to give reliable band structures, 75 we computed the electronic property of ph-BO using both PBE and HSE06 functionals by VASP code. For HSE computations, the random phase approximation (RPA) method was employed to compute the optical properties of ph-BO monolayer, the $9\times9\times1$ and $21\times21\times1$ k points were used for electronic and optical property calculations, respectively.

To examine the dynamic stability of ph-BO, we calculated the phonon dispersions at the PBE level of theory using ultrasoft pseudopotentials implemented in CASTEP code. A $2\times2\times1$ supercell, $13\times13\times1$ Monkhost-Pack k points, a cutoff of 500 eV, and 10^{-6} eV convergence tolerances were employed for phonon computations through finite displacement method.

To verify the thermal stability of our newly predicted monolayer, we performed *ab initio* molecular dynamics (AIMD) simulations using an all-electron method in DMol3 code since it is computationally less demanding.⁷⁷⁻⁷⁸ In AIMD simulations, the double numerical plus polarization (DNP) basis set and PBE functional were adopted; a 2×2×1 supercell was annealed using NVT canonical ensemble at different temperature of 500, 1000, 1500, and 2000 K, and each simulation lasted for 10 ps with a time step of 2.0 fs.

We also searched for the low-energy 2D planar BO monolayers using the

particle-swarm optimization (PSO) method as implemented in CALYPSO code.⁷⁹ The optimizations were performed by VASP code using PBE functional. In our calculations, the population size was set to 50, and the number of generation was set to 50. Unit cells containing 6 boron atoms and 6 oxygen atoms were considered.

3. Results and discussion

3.1 Geometric Structures

The optimization of lattice constant of ph-BO calculated is 7.82 Å (Figure S1). The optimized structure of ph-BO monolayer is purely planar, and has uniformly distributed pores with the pore diameter of 6.27 Å (Figure 1a). The B-O bond lengths are all 1.39 Å, and the B-B bonds are 1.72 Å, which are very close to those (1.385, 1.717 Å, respectively) in the planar $B_{10}O_{10}$ cluster composed by B_6O_6 dimers (named as B10-1 in Ref.70).

To scrutinize the bonding nature of ph-BO, we calculated its electron localization function (ELF). The ELF is a useful method to analyze the chemical bond classification through providing information about electron localization in molecules and solids. ELF can be described in the form of a contour pot in real space with values ranging from 0 to 1. The region with 1 indicates completely localization of electrons, 0 stands for a very low electron density area, while 0.5 indicates an area with homogenous electron gas. For ph-BO monolayer, the isosurface of ELF at 0.75 au is concentrated in two main parts: the middle of B-B bonds and the B-O bonds (especially around oxygen atoms) (Figure 2a). In the ELF sliced perpendicular to (001)

direction (Figure 2b), the values of the above mentioned two domains are larger than 0.8 au, which indicate that B-B and B-O are strong valence bonds, contributing to the durable *ph*-BO framework.

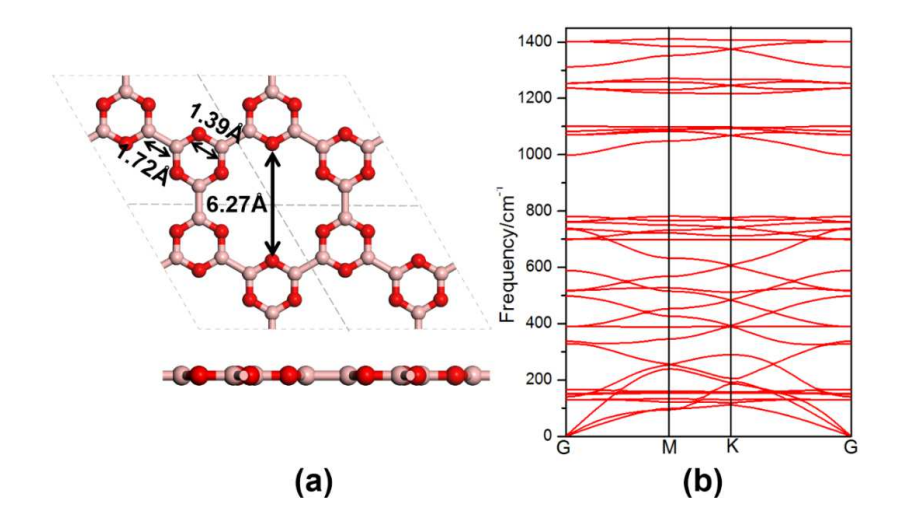


Figure 1. Top and side views (a) of geometric structure of ph-BO. The pink and red atoms represent B and O atoms. The B-O, B-B bond lengths are identical, respectively. For clarity, $(2 \times 2 \times 1)$ supercells are used here. Phonon dispersions (b) of the fully relaxed ph-BO monolayer structure.

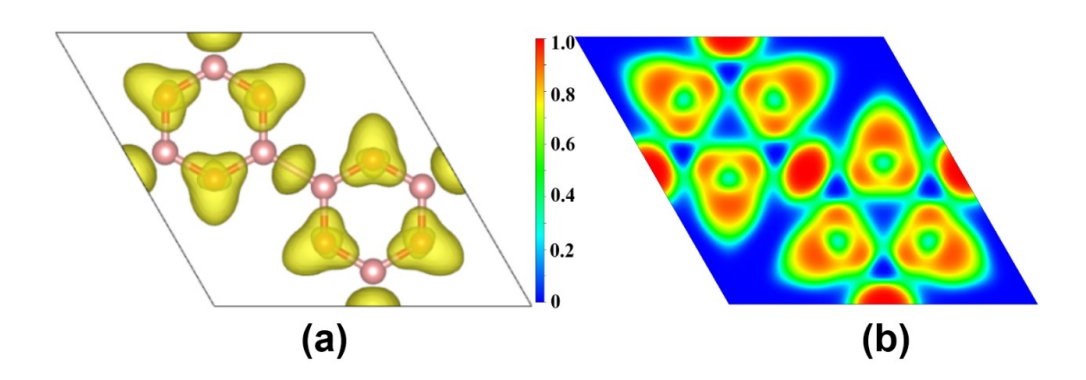


Figure 2. The isosurface of ELF plotted with a value of 0.75 au (a); and the ELF sliced perpendicular to (001) direction (b) for ph-BO monolayer.

Mechanical properties are important characteristics for a material, which can

help classify and identify materials. Thus, we also studied the mechanical properties of ph-BO through in-plane Young's modulus. Possessing hexagonal structures, the mechanical properties of ph-BO are isotropic, and the Young's modulus ($Y_a = Y_b$) of ph-BO is 71.83 N/m. For comparison, the Young's modulus of ph-BO is smaller than those of β_{12} borophene ($Y_a = 189$ N/m and $Y_b = 210$ N/m).⁵⁰ However, the Young's modulus of our newly predicted ph-BO is larger than that of silicene ($Y_a = Y_b = 60$ N/m),⁵⁰ and is comparable to those of phosphorene ($Y_a = 25.50$ N/m, $Y_b = 91.61$ N/m),⁸¹ suggesting that ph-BO has great mechanical property and potential in various nanoscale device applications.

3.2. Thermodynamic, Dynamic and Thermal Stabilities

The stability and the possibility of experimental realization are vital for any designed materials. Thus, we systematically evaluated the thermodynamic, dynamic and thermal stabilities of ph-BO monolayer.

First, we examined the thermodynamic stability of ph-BO monolayer by computing its binding energies (E_b) defined as

$$E_{\rm b} = (6E_{\rm B} + 6E_{\rm O} - E_{\rm BO}) / 12$$

Where E_B , E_O and E_{BO} are the total energies of the boron atom, oxygen atom and unit cell (One unit cell is composed of six boron and six oxygen atoms). The computed binding energy of ph-BO monolayer is 6.68 eV/atom. In comparison, the binding energies of the B_2O_3 monolayer with BO_3 and B_3O_6 triangle units (Figure S2) are 6.97 and 6.99 eV/atom, respectively. It is the presence of the B-B homo-element bonds that

lead to the slightly lower binding energy of ph-BO monolayer than the corresponding X_2O_3 2D structures. Compared with the 2D elemental layers, ph-BO has higher binding energy than χ_3 borophene (5.90 eV/atom)⁸² and β_{12} borophene (denoted $v_{1/6}$ -borophene) (5.89 eV/atom) at the same theoretical level.⁴⁹⁻⁵⁰ It is the strong covalent B-O bond that result in the high thermodynamic stabilities of the 2D boron oxide.

Secondly, we examined the dynamic stability of ph-BO monolayer by computing its phonon dispersions. The absence of imaginary frequency in the phonon dispersions (Figure 1b) confirm that ph-BO is dynamically stable.

We further examined the thermal stability of ph-BO by AIMD simulations (Figure 3). Fortunately, ph-BO monolayer well maintained its hexagonal structure at temperatures up to 1500 K. At 2000 K, the structure of ph-BO is corrupted with some broke B-B bonds. Note that ph-BO will have enough energy to cross the barrier and turn to disordered state at temperatures between 1500 and 2000 K. These simulations indicate that ph-BO monolayer has high thermal stability.

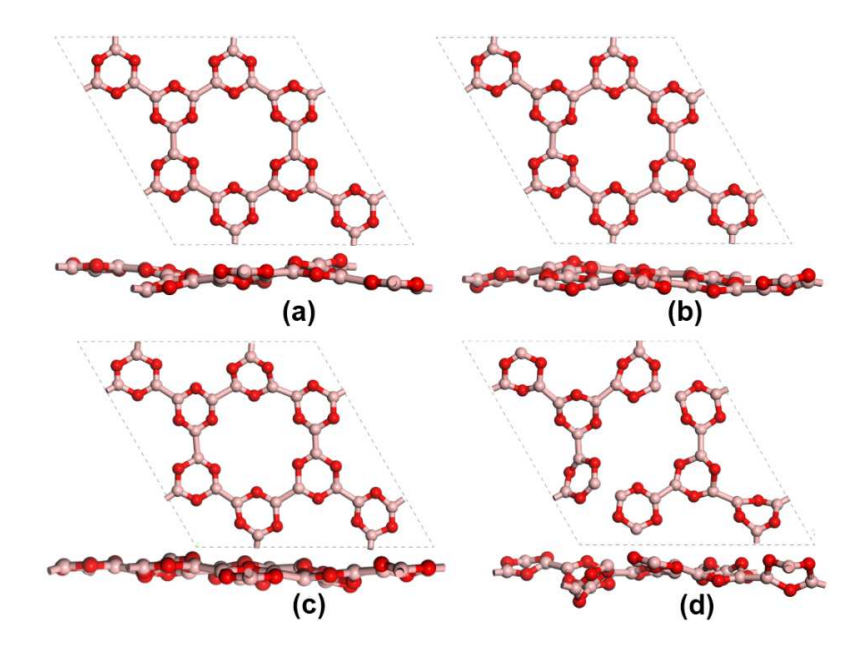


Figure 3. Snapshots of *ph*-BO equilibrium structures at (a) 500K, (b) 1000K, (c) 1500K and (d) 2000K at the end of 10 ps AIMD simulations.

Moreover, our PSO search revealed that the ph-BO monolayer as we designed is global minima of boron monoxide planar structures in 2D space. The other two low-lying energy boron monoxide, namely as BO-2 and BO-3 (Figure S4), have binding energies (6.64 and 6.62 eV/atom, respectively) 40 and 60 meV/atom smaller than ph-BO. Thus, the high thermodynamic, dynamic and thermal stabilities of ph-BO, as revealed by our computations of binding energies, phonon dispersions and AIMD simulations, strongly indicate that it is highly practicable to realize ph-BO experimentally.

3.3. Electronic properties

To study the electronic property of ph-BO, we computed its band structures as well as total and partial density of states (DOS and PDOS) (Figure 4). In band structures of ph-BO monolayer, there is no band lines across the Fermi level, wherein,

the conduction band minimum (CBM) is at K point (0.333, 0.333, 0), and valence band maximum (VBM) is at G point (0, 0, 0). Thus, ph-BO monolayer is semiconducting with indirect band gap of 3.59 (PBE). For comparison, the band gap of ph-BO (3.59 eV) is much smaller than those of the B_2O_3 monolayers with BO₃ and B_3O_6 triangle units (5.26 eV and 6.88 eV, respectively, computed at the same PBE level of theory in this work). Checking DOS and PDOS plots revealed that the bands close to the Fermi level are mainly attributed to the hybridization of p orbitals of boron and oxygen atoms.

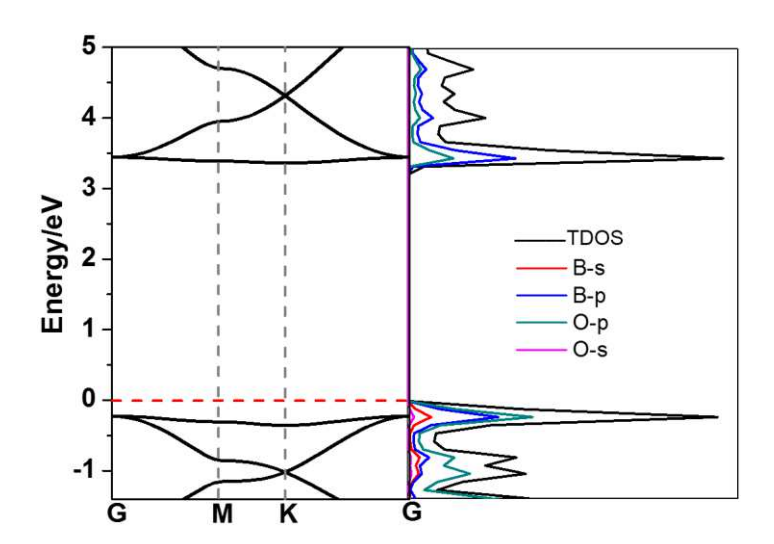


Figure 4. Band structures and partial density of states of *ph*-BO monolayer (by PBE functional).

Because the PBE functional tends to underestimate band gaps, we also employed HSE06 functional to get more accurate band gap value of ph-BO monolayer. The HSE06 band gaps for ph-BO is 5.23 eV, which correspond to UV range. Sharing similar electronic characteristics with hexagonal boron nitride (h-BN, band gap = 5.2-5.9 eV), $^{83-87}$ ph-BO monolayer is a typical wide band gap material, and is

expected to present emission/absorption wavelengths in the ultraviolet light.

Since the external strains are unavoidable, especially in the fabrication of nanostructures and thin films, we further studied the change of band gap values of ph-BO under in-plane biaxial strains. Though PBE underestimates the band gaps of semiconductors, the variation tendency is expected to be reliable. Therefore, the computations of strain effect were performed by PBE functional, under a constant unit cell with volume constraint; and the axial unit cell length l is determined by the percentage strain η ($l = l_0 (1 + \eta)$), where l_0 is the unit cell length of the optimized, unstrained nanostructure. Upon strains η ranging from -5% to 3% in the monolayer plane from a and b directions, the energy of ph-BO monolayer increases with the increasing compression or expansion strains (Figure S5). The indirect semiconductor characteristic of ph-BO monolayer persists, but the band gap values increase upon stretching, while decrease upon compressing (Figure 6). Under -5% to 3% strains, the band gaps of ph-BO monolayer change from 3.38 to 3.64 eV. The change upon strains in such a range is 0.26 eV for ph-BO monolayer, which indicates that the wide band gap character of ph-BO is rather robust against external strains.

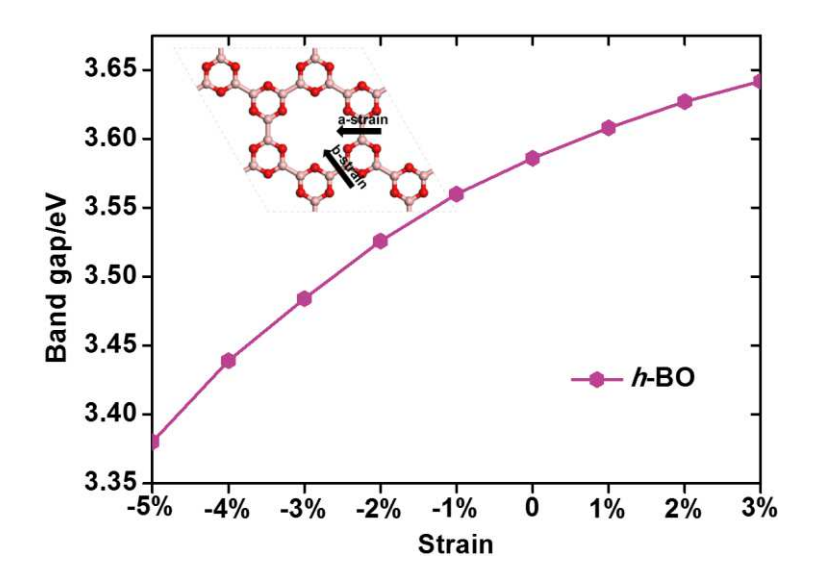


Figure 5. The change of band gap values under in-plane strain ranged from -5% to 3% with the view of the directions of strains.

3.4. Optical properties

The wide band gap of ph-BO suggests its promising applications in deep-UV range. To further explore its optical property, we computed the dielectric function of ph-BO. Herein, the transverse dielectric function $\varepsilon(\omega)$ below was used to describe the optical properties of materials.

$$\varepsilon(\omega) = \varepsilon_1(\omega) + i\varepsilon_2(\omega)$$

Where ω is the photon frequency, $\varepsilon_I(\omega)$ is the real part and $\varepsilon_2(\omega)$ is the imaginary part of dielectric function.

From the imaginary part of dielectric function, the curves of [100] and [010] are degenerate and dominant (Figure 6), and the threshold energy of dielectric function appear at around 5.13 eV. The threshold energy is close to the band gap value (both are in HSE06 theory level), which verifies the accuracy of our calculations. This peak corresponds to the optical transition between the top of valence band and bottom of

conduction band, which is called fundamental absorption edge. The predominant peaks for ph-BO monolayer from [100]/[010] orientation are at 7.46, 10.26, and 16.32 eV. Notably, the large area under the [100]/[010] curve (ca. 5-18 eV) indicate its high absorption coefficients in ultraviolet light range. Therefore, the prominent electronic and optical properties endow ph-BO highly promising as high-power electronics, blue light-emitting diodes (LED), deep-UV light emitters and blue-violet laser diodes. ⁸⁸⁻⁸⁹

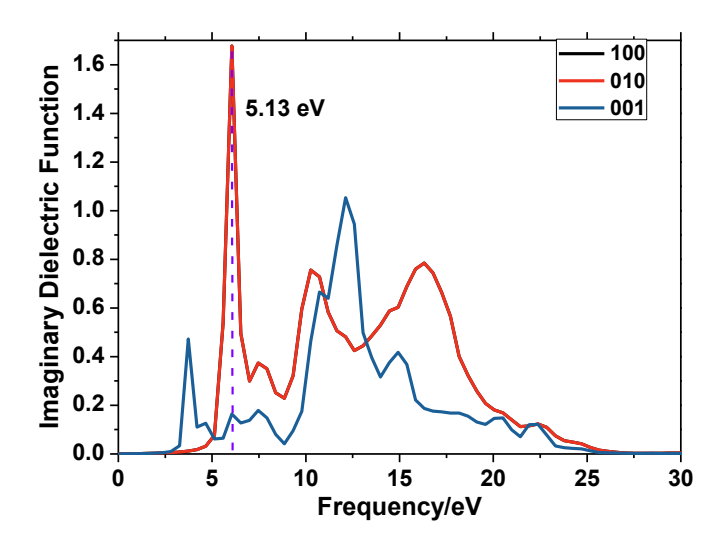


Figure 6. Imaginary parts of dielectric functions for *ph*-BO monolayer.

4. Conclusion

By means of systematic DFT computations, we designed a purely planar nanostructure with uniform pores, namely porous hexagonal boron oxide (*ph*-BO) monolayer. Due to strong B-O bonds, *ph*-BO monolayer has rather high stability, as illustrated by its high binding energy, absence of imaginary frequency dispersions, and well-maintained structure at high temperatures, which strongly indicate the feasibility for its experimental realization.

Notably, ph-BO monolayer is indirect semiconductor with rather wide band gap

comparable to hexagonal boron nitride, and its band gap is rather robust against

external strains. ph-BO monolayer has high absorption efficiencies in deep-UV light

range, which endow it great promise in electronics and optoelectronics, especially

high-power electronics, deep-UV light emitters and blue-violet laser diodes. We hope

that our newly designed ph-BO monolayer will inspire more efforts on 2D main group

oxide materials with wide band gaps.

Author Information

Corresponding Authors

Email: *zhongfangchen@gmail.com

ORCID

Zhongfang Chen: 0000-0002-1445-9184

Notes

The authors declare no competing financial interest.

Acknowledgement

This work was supported by the National Science Foundation-Centers of Research

Excellence in Science and Technology (NSF-CREST Center) for Innovation,

Research and Education in Environmental Nanotechnology (CIRE2N) (Grant No.

HRD-1736093) and NASA (Grant No. 17-EPSCoRProp-0032). We greatly appreciate

the technical supports in the High Performance Computational facility (HPCf) at

University of Puerto Rico.

16

Supporting Information

The optimization of lattice constant of *ph*-BO monolayer; optimized structures of the sublattices of the B₂O₃ polymorphs with (a) BO₃ and (b) B₃O₆ triangle units; change of total energy and temperature of *ph*-BO during 10 ps AIMD simulations at 1500 K; change of total energies of *ph*-BO under in-plane biaxial strain ranged from -5% to 3% (VASP package, PBE functional). This material is available free of charge via the Internet at https://doi.org.

References

- Novoselov, K. S.; Geim, A. K.; Morozov, S. V.; Jiang, D.; Zhang, Y.; Dubonos, S. V.; Grigorieva, I. V.; Firsov, A. A. Electric Field Effect in Atomically Thin Carbon Films. *Science* 2004, 306, 666-9.
- 2. Molle, A.; Goldberger, J.; Houssa, M.; Xu, Y.; Zhang, S. C.; Akinwande, D. Buckled Two-Dimensional Xene Sheets. *Nat. Mater.* **2017**, *16*, 163-169.
- 3. Tang, Q.; Zhou, Z. Graphene-Analogous Low-Dimensional Materials. *Prog. Mater. Sci.* **2013**, *58*, 1244-1315.
- 4. Novoselov, K. S.; Mishchenko, A.; Carvalho, A.; Castro Neto, A. H. 2D Materials and Van Der Waals Heterostructures. *Science* **2016**, *353*, aac9439.
- Balendhran, S.; Walia, S.; Nili, H.; Sriram, S.; Bhaskaran, M. Elemental
 Analogues of Graphene: Silicene, Germanene, Stanene, and Phosphorene. *Small* 2015,
 640-52.
- 6. Xu, M.; Liang, T.; Shi, M.; Chen, H. Graphene-Like Two-Dimensional Materials.

- Chem. Rev. 2013, 113, 3766-98.
- 7. Wang, G.; Pandey, R.; Karna, S. P., Atomically thin group V elemental films: theoretical investigations of antimonene allotropes. *ACS Appl. Mater. & Inter.*, **2015**, *7*, 11490-11496.
- 8. Kou, L.; Chen, C.; Smith, S. C. Phosphorene: Fabrication, Properties, and Applications. *J. Phys. Chem. Lett.* **2015**, *6*, 2794-805.
- 9. Butler, S. Z., et al. Progress, Challenges, and Opportunities in Two-Dimensional Materials Beyond Graphene. *ACS Nano* **2013**, *7*, 2898-926.
- 10. Tang, Q.; Zhou, Z.; Chen, Z. F. Innovation and Discovery of Graphene-Like Materials Via Density-Functional Theory Computations. *Wires. Comput. Mol. Sci.* **2015**, *5*, 360-379.
- 11. Zhao, J. J., et al. Rise of Silicene: A Competitive 2D Material. *Prog. Mater. Sci.* **2016**, *83*, 24-151.
- 12. Guzmán-Verri, G. G.; Lew Yan Voon, L. C. Electronic Structure of Silicon-Based Nanostructures. *Phys. Rev. B* **2007**, *76*, 075131.
- 13. Chen, L.; Liu, C. C.; Feng, B.; He, X.; Cheng, P.; Ding, Z.; Meng, S.; Yao, Y.; Wu, K. Evidence for Dirac Fermions in a Honeycomb Lattice Based on Silicon. *Phys. Rev. Lett.* **2012**, *109*, 056804.
- 14. De Padova, P.; Vogt, P.; Resta, A.; Avila, J.; Razado-Colambo, I.; Quaresima, C.; Ottaviani, C.; Olivieri, B.; Bruhn, T.; Hirahara, T. Evidence of Dirac Fermions in Multilayer Silicene. *Appl. Phys. Lett.* **2013**, *102*, 163106.
- 15. Durgun, E.; Tongay, S.; Ciraci, S. Silicon and III-V Compound Nanotubes:

- Structural and Electronic Properties. *Phys. Rev. B* **2005**, *72*, 075420.
- 16. Rothlisberger, U.; Andreoni, W.; Parrinello, M. Structure of Nanoscale Silicon Clusters. *Phys. Rev. Lett.* **1994**, *72*, 665-668.
- 17. Vogt, P.; De Padova, P.; Quaresima, C.; Avila, J.; Frantzeskakis, E.; Asensio, M. C.; Resta, A.; Ealet, B.; Le Lay, G. Silicene: Compelling Experimental Evidence for Graphenelike Two-Dimensional Silicon. *Phys. Rev. Lett.* **2012**, *108*, 155501.
- 18. Cahangirov, S.; Audiffred, M.; Tang, P.; Iacomino, A.; Duan, W.; Merino, G.; Rubio, A., Electronic Structure of Silicene on Ag (111): Strong Hybridization Effects. *Phys. Rev. B*, **2013**, *88*, 035432
- 19. Cahangirov, S.; Topsakal, M.; Akturk, E.; Sahin, H.; Ciraci, S. Two- and One-Dimensional Honeycomb Structures of Silicon and Germanium. *Phys. Rev. Lett.* **2009**, *102*, 236804.
- 20. Takeda, K.; Shiraishi, K. Theoretical Possibility of Stage Corrugation in Si and Ge Analogs of Graphite. *Phys. rev. B: Condens. Matter Mater. Phys.* **1994**, *50*, 14916-14922.
- 21. Jing, Y.; Zhou, Z.; Cabrera, C. R.; Chen, Z. F. Graphene, Inorganic Graphene Analogs and Their Composites for Lithium Ion Batteries. *J. Mater. Chem. A* **2014**, *2*, 12104-12122.
- 22. Dávila, M.; Xian, L.; Cahangirov, S.; Rubio, A.; Le Lay, G. Germanene: A Novel Two-Dimensional Germanium Allotrope Akin to Graphene and Silicene. *New J. Phys.* **2014**, *16*, 095002.
- 23. Houssa, M.; Scalise, E.; Sankaran, K.; Pourtois, G.; Afanas'ev, V. V.; Stesmans, A.

Electronic Properties of Hydrogenated Silicene and Germanene. *Appl. Phys. Lett.* **2011**, *98*, 223107.

- 24. Li, L.; Lu, S. Z.; Pan, J.; Qin, Z.; Wang, Y. Q.; Wang, Y.; Cao, G. Y.; Du, S.; Gao, H. J. Buckled Germanene Formation on Pt(111). *Adv. Mater.* **2014**, *26*, 4820-4.
- 25. Zhu, F. F.; Chen, W. J.; Xu, Y.; Gao, C. L.; Guan, D. D.; Liu, C. H.; Qian, D.; Zhang, S. C.; Jia, J. F. Epitaxial Growth of Two-Dimensional Stanene. *Nat. Mater.* **2015**, *14*, 1020-5.
- 26. Tang, P. Z.; Chen, P. C.; Cao, W. D.; Huang, H. Q.; Cahangirov, S.; Xian, L. D.; Xu, Y.; Zhang, S. C.; Duan, W. H.; Rubio, A. Stable Two-Dimensional Dumbbell Stanene: A Quantum Spin Hall Insulator. *Phys. Rev. B* **2014**, *90*, 121408.
- 27. Rachel, S.; Ezawa, M. Giant Magnetoresistance and Perfect Spin Filter in Silicene, Germanene, and Stanene. *Phys. Rev. B* **2014**, *89*, 195303.
- 28. Gao, N.; Liu, H. S.; Zhou, S.; Bai, Y. Z.; Zhao, J. J. Interaction between Post-Graphene Group-IV Honeycomb Monolayers and Metal Substrates: Implication for Synthesis and Structure Control. *J. Phys. Chem. C* **2017**, *121*, 5123-5129.
- 29. Li, L.; Yu, Y.; Ye, G. J.; Ge, Q.; Ou, X.; Wu, H.; Feng, D.; Chen, X. H.; Zhang, Y. Black Phosphorus Field-Effect Transistors. *Nat. Nanotechnol.* **2014**, *9*, 372-7.
- 30. Churchill, H. O.; Jarillo-Herrero, P. Two-Dimensional Crystals: Phosphorus Joins the Family. *Nat. Nanotechnol.* **2014**, *9*, 330-1.
- 31. Liu, H.; Neal, A. T.; Zhu, Z.; Tomanek, D.; Ye, P. D. Phosphorene: A New 2D Material with High Carrier Mobility. *arXiv preprint arXiv:1401.4133* **2014**.
- 32. Carvalho, A.; Wang, M.; Zhu, X.; Rodin, A. S.; Su, H. B.; Neto, A. H. C.

- Phosphorene: From Theory to Applications. *Nature Reviews Materials* **2016**, *1*, 16061.
- 33. Jing, Y.; Zhang, X.; Zhou, Z. Phosphorene: What Can We Know from Computations? *Wires. Comput. Mol. S.* **2016**, *6*, 5-19.
- 34. Fei, R.; Yang, L. Strain-Engineering the Anisotropic Electrical Conductance of Few-Layer Black Phosphorus. *Nano Lett.* **2014**, *14*, 2884-9.
- 35. Wang, L.; Kutana, A.; Zou, X.; Yakobson, B. I. Electro-Mechanical Anisotropy of Phosphorene. *Nanoscale* **2015**, *7*, 9746-51.
- 36. Zhang, S.; Yan, Z.; Li, Y.; Chen, Z.; Zeng, H. Atomically Thin Arsenene and Antimonene: Semimetal-Semiconductor and Indirect-Direct Band-Gap Transitions. *Angew. Chem., Int. Ed. Engl.* **2015**, *54*, 3112-5.
- 37. Tsai, H. S.; Wang, S. W.; Hsiao, C. H.; Chen, C. W.; Ouyang, H.; Chueh, Y. L.; Kuo, H. C.; Liang, J. H. Direct Synthesis and Practical Bandgap Estimation of Multilayer Arsenene Nanoribbons. *Chem. Mater.* **2016**, *28*, 425-429.
- 38. Zhang, S.; Xie, M.; Li, F.; Yan, Z.; Li, Y.; Kan, E.; Liu, W.; Chen, Z.; Zeng, H. Semiconducting Group 15 Monolayers: A Broad Range of Band Gaps and High Carrier Mobilities. *Angew. Chem., Int. Ed. Engl.* **2016**, *55*, 1666-9.
- 39. Tsai, H. S.; Chen, C. W.; Hsiao, C. H.; Ouyang, H.; Liang, J. H. The Advent of Multilayer Antimonene Nanoribbons with Room Temperature Orange Light Emission. *Chem. Commun. (Camb)* **2016**, *52*, 8409-12.
- 40. Ares, P.; Aguilar-Galindo, F.; Rodriguez-San-Miguel, D.; Aldave, D. A.; Diaz-Tendero, S.; Alcami, M.; Martin, F.; Gomez-Herrero, J.; Zamora, F. Mechanical

- Isolation of Highly Stable Antimonene under Ambient Conditions. *Adv. Mater.* **2016**, 28, 6332-6336.
- 41. Gibaja C., Rodriguez San Miguel D., Ares P., et al. Few-Layer Antimonene by Liquid-Phase Exfoliation. *Angew. Chem., Int. Ed. Engl.* **2016**, *55*, 14345-14349.
- 42. Ji J., Song X., Liu J., et al. Two-Dimensional Antimonene Single Crystals Grown by Van Der Waals Epitaxy. *Nat. Commun.* **2016**, *7*, 13352.
- 43. Tang, H.; Ismail-Beigi, S. Novel Precursors for Boron Nanotubes: The Competition of Two-Center and Three-Center Bonding in Boron Sheets. *Phys. Rev. Lett.* **2007**, *99*, 115501.
- 44. Galeev, T. R.; Chen, Q.; Guo, J. C.; Bai, H.; Miao, C. Q.; Lu, H. G.; Sergeeva, A. P.; Li, S. D.; Boldyrev, A. I. Deciphering the Mystery of Hexagon Holes in an All-Boron Graphene Alpha-Sheet. *Phys. Chem. Chem. Phys.* **2011**, *13*, 11575-8.
- 45. Wu, X.; Dai, J.; Zhao, Y.; Zhuo, Z.; Yang, J.; Zeng, X. C. Two-Dimensional Boron Monolayer Sheets. *ACS Nano* **2012**, *6*, 7443-53.
- 46. Penev, E. S.; Bhowmick, S.; Sadrzadeh, A.; Yakobson, B. I. Polymorphism of Two-Dimensional Boron. *Nano Lett.* **2012**, *12*, 2441-5.
- 47. Yu, X.; Li, L. L.; Xu, X. W.; Tang, C. C., Prediction of Two-Dimensional Boron Sheets by Particle Swarm Optimization Algorithm. *J. Phys. Chem. C* **2012**, *116*, 20075-20079.
- 48. Zhang, Z.; Yang, Y.; Gao, G.; Yakobson, B. I. Two-Dimensional Boron Monolayers Mediated by Metal Substrates. *Angew. Chem., Int. Ed. Engl.* **2015**, *54*, 13022-6.

- 49. Zhang, Z.; Mannix, A. J.; Hu, Z.; Kiraly, B.; Guisinger, N. P.; Hersam, M. C.; Yakobson, B. I. Substrate-Induced Nanoscale Undulations of Borophene on Silver. *Nano Lett.* **2016**, *16*, 6622-6627.
- 50. Zhang, Z. H.; Yang, Y.; Penev, E. S.; Yakobson, B. I. Elasticity, Flexibility, and Ideal Strength of Borophenes. *Adv. Funct. Mater.* **2017**, *27*.
- 51. Feng, B.; Zhang, J.; Zhong, Q.; Li, W.; Li, S.; Li, H.; Cheng, P.; Meng, S.; Chen, L.; Wu, K. Experimental Realization of Two-Dimensional Boron Sheets. *Nat. Chem.* **2016**, *8*, 563-8.
- 52. Mannix, A. J., et al. Synthesis of Borophenes: Anisotropic, Two-Dimensional Boron Polymorphs. *Science* **2015**, *350*, 1513-6.
- 53. Hall, H. T.; Compton, L. A. Group IV Analogs and High Pressure, High Temperature Synthesis of B₂O. *Inorg. Chem.* **1965**, *4*, 1213-1216.
- 54. Endo, T.; Sato, T.; Shimada, M. High-Pressure Synthesis of B₂O with Diamond-Like Structure. *J. Mater. Sci. Lett.* **1987**, *6*, 683-685.
- 55. Solozhenko, V. L.; Kurakevych, O. O.; Turkevich, V. Z.; Turkevich, D. V. Phase Diagram of the β-B₂O₃ System at 5 Gpa: Experimental and Theoretical Studies. *J. Phys. Chem. B* **2008**, *112*, 6683-7.
- 56. Grumbach, M. P.; Sankey, O. F.; McMillan, P. F. Properties of B₂O: An Unsymmetrical Analog of Carbon. *Phys. Rev. B* **1995**, *52*, 15807-15811.
- 57. He, D. W.; Zhao, Y. S.; Daemen, L.; Qian, J.; Shen, T. D.; Zerda, T. W. Boron Suboxide: As Hard as Cubic Boron Nitride. *Appl. Phys. Lett.* **2002**, *81*, 643-645.
- 58. Hwang, S. J.; Fernandez, C.; Amoureux, J. P.; Cho, J.; Martin, S. W.; Pruski, M.

- Quantitative Study of the Short Range Order in B₂O₃ and B₂S₃ by Mas and Two-Dimensional Triple-Quantum MAS ¹¹B NMR. *Solid State Nucl. Mag.* **1997**, 8, 109-21.
- 59. Ferlat, G.; Seitsonen, A. P.; Lazzeri, M.; Mauri, F. Hidden Polymorphs Drive Vitrification in B₂O₃. *Nat. Mater.* **2012**, *11*, 925-9.
- 60. Youngman, R. E.; Haubrich, S. T.; Zwanziger, J. W.; Janicke, M. T.; Chmelka, B.
 F. Short-and Intermediate-Range Structural Ordering in Glassy Boron Oxide. *Science*1995, 269, 1416-20.
- 61. Aziz, M. J.; Nygren, E.; Hays, J. F.; Turnbull, D. Crystal-Growth Kinetics of Boron-Oxide under Pressure. *J. Appl. Phys.* **1985**, *57*, 2233-2242.
- 62. Putkonen, M.; Niinistö, L., Atomic Layer Deposition of B₂O₃ Thin Films at Room Temperature. *Thin Solid Films*, **2006**, *514*, 145-149.
- 63. Ma, R.; Bando, Y., Self-Assembled Array of Boron Oxide Nanowires on Mg Surface. *Chem. Phys. Lett.*, **2003**, *374*, 358-361.
- 64. Cao, L.; Zhang, Z.; Sun, L.; Gao, C.; He, M.; Wang, Y.; Li, Y.; Zhang, X.; Li, G.; Zhang, J., Well Aligned Boron Nanowire Arrays. *Adv. Mater.*, **2001**, *13*, 1701-1704.
- 65. Chen, H.; Tan, J.; Cui, J.; Yang, X.; Zheng, H.; Zhu, Y.; Li, Y., Promoting Effect of Boron Oxide on Ag/SiO₂ Catalyst for the Hydrogenation of Dimethyl Oxalate to Methyl Glycolate. *Mol. Catal.*, **2017**, *433*, 346-353.
- 66. Ishak, R.; Picard, D.; Laroche, G.; Ziegler, D. P.; Alamdari, H., Application of Boron Oxide as a Protective Surface Treatment to Decrease the Air Reactivity of Carbon Anodes. *Metals*, **2017**, *7*, 79.

- 67. Claeyssens, F.; Allan, N. L.; Norman, N. C.; Russell, C. A., Design of Three-Dimensional Solid-State Boron Oxide Networks: Ab Initio Calculations Using Density Functional Theory., *Phys. Rev. B*, **2010**, *82*, 094119.
- 68. Zhang, Z.; Pu, L.; Li, Q. S.; King, R. B., Pathways to the Polymerization of Boron Monoxide Dimer to Give Low-Density Porous Materials Containing Six-Membered Boroxine Rings. *Inorg. Chem.* **2015**, *54*, 2910-5.
- 69. Tian, W.-J.; Tian, X.-X.; Mu, Y.-W.; Lu, H.-G.; Li, S.-D., Double-Ring Tubular (B₂O₂) N Clusters (N= 6–42) Rolled up from the Most Stable BO Double-Chain Ribbon in Boron Monoxides., *Phys. Chem. Chem. Phys.*, **2017**, *19*, 23213-23217.
- 70. Liu, Y.; Liu, C.; Pu, L.; Zhang, Z.; King, R., Boron Monoxide Dimer as a Building Block for Boroxine Based Buckyballs and Related Cages: A Theoretical Study. *Chem. Commun.* **2017**, *53*, 3239-3241.
- 71. Zhang, R.; Li, Z.; Yang, J., Two-Dimensional Stoichiometric Boron Oxides as a Versatile Platform for Electronic Structure Engineering. *J. Phys. Chem. Lett.*, **2017**, *8*, 4347-4353.
- 72. Blöchl, P. E. Projector Augmented-Wave Method. *Phys. rev. B: Condens. Matter Mater. Phys.* **1994**, *50*, 17953-17979.
- 73. Kresse, G.; Hafner, J. Ab Initio Molecular Dynamics for Liquid Metals. *Phys. rev. B. Condens. Matter Mater. Phys.* **1993**, *47*, 558-561.
- 74. Heyd, J.; Scuseria, G. E.; Ernzerhof, M. Hybrid Functionals Based on a Screened Coulomb Potential. *J. Chem. Phys.* **2003**, *118*, 8207-8215.
- 75. Filippi, C.; Singh, D. J.; Umrigar, C. J. All-Electron Local-Density and

- Generalized-Gradient Calculations of the Structural Properties of Semiconductors. *Phys rev. B. Condens. Matter Mater. Phys.* **1994**, *50*, 14947-14951.
- 76. Segall, M. D.; Lindan, P. J. D.; Probert, M. J.; Pickard, C. J.; Hasnip, P. J.; Clark,S. J.; Payne, M. C. First-Principles Simulation: Ideas, Illustrations and the Castep
- Code. J. Phys.: Condens. Matter 2002, 14, 2717-2744.
- 77. Delley, B. An All-Electron Numerical-Method for Solving the Local Density Functional for Polyatomic-Molecules. *J. Chem. Phys.* **1990**, *92*, 508-517.
- 78. Delley, B. From Molecules to Solids with the Dmol3 Approach. *J. Chem. Phys.* **2000**, *113*, 7756-7764.
- 79. Wang, Y.; Lv, J.; Zhu, L.; Ma, Y., Crystal Structure Prediction Via Particle-Swarm Optimization., *Phys. Rev. B*, **2010**, *82*, 094116.
- 80. Savin, A.; Nesper, R.; Wengert, S.; Fassler, T. F. Elf: The Electron Localization Function. *Angew. Chem., Int. Ed.* **1997**, *36*, 1809-1832.
- 81. Wang, Y.; Li, F.; Li, Y.; Chen, Z. Semi-Metallic Be₅C₂ Monolayer Global Minimum with Quasi-Planar Pentacoordinate Carbons and Negative Poisson's Ratio. *Nat. Commun.* **2016**, *7*, 11488.
- 82. Peng, B.; Zhang, H.; Shao, H.; Ning, Z.; Xu, Y.; Ni, G.; Lu, H.; Zhang, D. W.; Zhu, H. Stability and Strength of Atomically Thin Borophene from First Principles Calculations. *Mater. Res. Lett.* **2017**, 1-9.
- 83. Blase, X.; Rubio, A.; Louie, S. G.; Cohen, M. L. Quasiparticle Band Structure of Bulk Hexagonal Boron Nitride and Related Systems. *Phys. rev. B: Condens. Matter Mater. Phys.* **1995**, *51*, 6868-6875.

- 84. Hoffman, D.; Doll, G.; Eklund, P. Optical Properties of Pyrolytic Boron Nitride in the Energy Range 0.05—10 eV. *Phys. Rev. B* **1984**, *30*, 6051.
- 85. Watanabe, K.; Taniguchi, T.; Kanda, H. Direct-Bandgap Properties and Evidence for Ultraviolet Lasing of Hexagonal Boron Nitride Single Crystal. *Nat. Mater.* **2004**, *3*, 404-9.
- 86. Golberg, D.; Bando, Y.; Huang, Y.; Terao, T.; Mitome, M.; Tang, C.; Zhi, C. Boron Nitride Nanotubes and Nanosheets. *ACS nano* **2010**, *4*, 2979-2993.
- 87. Pakdel, A.; Bando, Y.; Golberg, D. Nano Boron Nitride Flatland. *Chem. Soc. Rev.* **2014**, *43*, 934-959.
- 88. Kubota, Y.; Watanabe, K.; Tsuda, O.; Taniguchi, T. Deep Ultraviolet Light-Emitting Hexagonal Boron Nitride Synthesized at Atmospheric Pressure. *Science* **2007**, *317*, 932-934.
- 89. Takahashi, K.; Yoshikawa, A.; Sandhu, A. Wide Bandgap Semiconductors. Springer-Verlag Berlin Heidelberg. **2007**, 239.